Soft Matter

ARTICLE TYPE

Cite this: DOI: 00.0000/xxxxxxxxxx

Data-driven Coarse-grained Modeling of Non-equilibrium Systems†

Shu Wang,[a‡] Zhan Ma,[a‡] and Wenxiao Pan[a*]

Received Date
Accepted Date

DOI: 00.0000/xxxxxxxxxx

Modeling a high-dimensional Hamiltonian system in reduced dimensions with respect to coarse-grained (CG) variables can greatly reduce computational cost and enable efficient bottom-up prediction of main features of the system for many applications. However, it usually experiences significantly altered dynamics due to loss of degrees of freedom upon coarse-graining. To establish CG models that can faithfully preserve dynamics, previous efforts mainly focused on equilibrium systems. In contrast, various soft matter systems are known out of equilibrium. Therefore, the present work concerns non-equilibrium systems and enables accurate and efficient CG modeling that preserves non-equilibrium dynamics and is generally applicable to any non-equilibrium process and any observable of interest. To this end, the dynamic equation of a CG variable is built in the form of the non-stationary generalized Langevin equation (nsGLE) to account for the dependence of non-equilibrium processes on the initial conditions, where the two-time memory kernel is determined from the data of the two-time auto-correlation function of the non-equilibrium trajectory-averaged observable of interest. By embedding the non-stationary non-Markovian process in an extended stochastic framework, an explicit form of the non-stationary random noise in the nsGLE is introduced, and the cost is significantly reduced for solving the nsGLE to predict the non-equilibrium dynamics of the CG variable. To prove and exploit the equivalence of the nsGLE and extended dynamics, the memory kernel is parameterized in a two-time exponential expansion. A data-driven hybrid optimization process is proposed for the parameterization, which integrates the differential-evolution method with the Levenberg–Marquardt algorithm to efficiently tackle a non-convex and high-dimensional optimization problem.

1 Introduction

For a system of many degrees of freedom evolving according to Hamiltonian equations of motion, it is often practical to describe a process of interest with respect to the evolution of a small set of relevant observables (“coarse-grained" variables) that capture the main features of the process. For example, considering a system of biomolecules or proteins, one is interested in the collective motion of specific groups of atoms to understand a biological mechanism[1–3]; chemical reactions and phase transitions are usually characterized in terms of reaction coordinates[4]. In these examples, it is useful to construct the equation of motion that precisely governs the dynamics of reduced-dimension coarse-grained (CG) variables. In the context of computer simulations, a full molecular dynamics (MD) simulation for a complex many-body system is usually computationally demanding, but solving a reduced-dimension equation can be more efficient. Such equation can be established by systematically integrating out “irrelevant" degrees of freedom such as detailed information of the molecules and/or the solvent surrounding the molecules. Along this line, most previous studies concentrated on systems at equilibrium, where the generalized Langevin equation (GLE)[5,6] has been established to describe the equilibrium dynamics of CG variables and applied in various CG models[7–13]. However, many soft matter systems are known out of equilibrium, e.g., molecular self-assembly driven by time-dependent temperature protocols[14–17], dynamics of DNA under an applied force[18], and polymer dynamics in a flow[19]. Therefore, it is of more interest in practice to be able to properly describe the non-equilibrium dynamics of CG variables. To this end, the non-stationary generalized Langevin equation (nsGLE)[4,20] has recently been established as a promising mathematical framework for CG modeling of non-equilibrium systems, which provides the equation of motion for the CG variables subject to non-equilibrium processes. In principle, the nsGLE can be rigorously derived using time-dependent projection operators[20,21]. It does not require time scale separation, i.e., the CG variable can be any observable of interest, whether slow or fast relative to the dynamics of unresolved degrees of freedom.

[a] Department of Mechanical Engineering, University of Wisconsin-Madison, Madison, WI 53706.

* Corresponding author. E-mail: wpan9@wisc.edu

† Electronic Supplementary Information (ESI) available. See DOI: 10.1039/cXsm00000x/

‡ These authors contributed equally to this work

Similarly to the GLE, the nsGLE implicitly incorporates the kinetic effects of unresolved degrees of freedom through a memory term and a random noise term. However, different from the GLE, the memory kernel in the nsGLE is a two-time function to account for the dependence on the initial conditions of non-equilibrium processes. Although theoretically sound, applying the nsGLE to practical CG modeling encounters the following challenges. First, the memory function must be specified. It can involve solving an ill-posed inverse problem, which requires proper regularization to ensure a stable solution. In literature, the non-stationary memory kernel was determined through an iterative procedure[22], which is computationally expensive and cannot address the ill-posedness of the problem. Second, since the non-stationary memory kernel is a two-time function, giving an explicit form of the random noise such that the memory and random noise obey a fluctuation-dissipation like relation is a challenging task, which has not been resolved in previous studies[4,20]. Third, once the memory kernel and random noise are specified, the nsGLE can be solved to predict the dynamics of CG variables in a non-equilibrium process. However, directly solving the nsGLE can be computationally expensive because the convolution of memory requires the historical information of CG variables at every time step, and the random term requires sampling colored noise, which makes the CG modeling based on the nsGLE not so efficient as expected theoretically.

The present work aims to address the challenges of applying the nsGLE to CG modeling of non-equilibrium systems, and our contributions include the following. First, we propose a numerical method that can efficiently and stably determine the memory kernel from the data of the two-time auto-correlation function of the non-equilibrium trajectory-averaged observable of interest. For prediction beyond the range of the data set, the memory kernel is extrapolated via the Gaussian process regression. Second, by approximating the memory kernel in a two-time exponential expansion, we prove the equivalence of the nsGLE and an extended Markovian process, which represents the first attempt to generalize the framework of extended dynamics for non-stationary non-Markovian processes. By embedding the nsGLE in an extended dynamics framework, we are able to give the explicit form of the random noise and in the meanwhile to avoid the expensive convolution of memory, rendering the CG modeling computationally tractable. Third, to parameterize the exponential expansion approximating the memory kernel, we propose a systematic approach via data-driven optimization. In particular, we propose a hybrid optimization process that leverages the differential-evolution and Levenberg–Marquardt algorithms for non-convex and high-dimensional optimization. Finally, for validation, we apply the proposed methodology to a representative non-equilibrium system: a star-polymer melt in a heating process. Star-polymer melts have been used as typical benchmark systems for validating CG models[7,9,23,24]. The methodology proposed in this work is applicable to CG modeling of various non-equilibrium soft matter systems, for which only data accessible in either simulations or experiments for the reference Hamiltonian system are needed.

2 Non-stationary generalized Langevin equation

Without loss of generality, we denote a CG coordinate (mass-scaled) as $\hat{\mathbf{R}}(t)$ of d dimension and the corresponding momentum as $\hat{\mathbf{P}}(t)$. The nsGLE can then be written as[20]:

$$\frac{d\hat{\mathbf{P}}(t)}{dt} = \langle \hat{\mathbf{F}}(t) \rangle - \int_0^t dt' \hat{K}(t',t)\hat{\mathbf{P}}(t') + \hat{\tilde{\mathbf{F}}}(t) \,, \tag{1}$$

where the three terms in the right-hand side correspond to the mean force, a friction term, and a random noise term, respectively; and $\langle\cdot\rangle$ represents the trajectory average taken over an ensemble of dynamic trajectories. This equation is similar in structure to the GLE but exhibits a two-time memory kernel $\hat{K}(t',t)$ and a random force $\hat{\tilde{\mathbf{F}}}$ that implicitly depend on the initial conditions of the process. If we choose the normalized momentum $\mathbf{P}(t) = \frac{\hat{\mathbf{P}}(t) - \langle \hat{\mathbf{P}}(t) \rangle}{\sqrt{\langle |\hat{\mathbf{P}}(t)|^2 \rangle - \langle \hat{\mathbf{P}}(t) \rangle^2}}$ as the CG variable, the nsGLE can be simplified as:

$$\frac{d\mathbf{P}(t)}{dt} = -\int_0^t dt' K(t',t)\mathbf{P}(t') + \tilde{\mathbf{F}}(t) \,. \tag{2}$$

The memory kernel and random force satisfy:

$$K(t',t) = \frac{\langle \tilde{\mathbf{F}}(t') \cdot \tilde{\mathbf{F}}(t) \rangle}{\langle |\mathbf{P}(t')|^2 \rangle} \,, \tag{3}$$

which is analogous to the fluctuation-dissipation relation for equilibrium dynamics[25] but holds for non-stationary processes[4].

2.1 Determine the memory kernel

To determine the two-time memory kernel $K(t',t)$, we rely on the property that the momentum $\mathbf{P}(t')$ and the random force $\tilde{\mathbf{F}}(t)$ come from two orthogonal sub-spaces, and hence $\langle \mathbf{P}(t') \cdot \tilde{\mathbf{F}}(t) \rangle = 0$. Multiplying both sides of Eq. (2) by $\mathbf{P}(t')$ and taking the trajectory-average lead to:

$$-D(t',t) = \int_{t'}^t C(t',t'')K(t'',t)dt'' \,, \tag{4}$$

with the two-time auto-correlation function of momentum $C(t',t) = \langle \mathbf{P}(t') \cdot \mathbf{P}(t) \rangle$ and the force-momentum correlation function $D(t',t) = \frac{\partial C(t',t)}{\partial t}$. The memory kernel $K(t',t)$ can then be determined via deconvolution of Eq. (4) given $C(t',t)$ and $D(t',t)$. Note that the integral operator in equation (4) is the adjoint of Volterra operator[26]. Although the deconvolution can have a unique continuous solution, the solution does not depend continuously on the data; i.e., the solution is unstable against data noise, due to the nondegeneracy of $C(t',t)$. Thus, solving the deconvolution to determine the memory kernel is an ill-posed problem, and proper regularization must be enforced. In practice, what we have are the data of $C(t',t)$ and $D(t',t)$ at discrete time instances, and hence, the deconvolution can be solved in the discrete setting. Note that discretization can regularize the ill-posed deconvolution problem, known as the "self-regularization" property of discretization[27]. After discretization, the deconvolution becomes well-posed, but the resulting linear problem could be ill-conditioned[28] and require further regularization, for which the Tikhonov regularization[29,30] is adopted in this work.

Applying the midpoint quadrature rule[26], Eq. (4) can be discretized into the following linear system:

$$\Delta t \mathbf{C}_n \mathbf{K}_n = -\mathbf{D}_n \tag{5}$$

for every discrete time $t_n = n\Delta t$, where $\mathbf{C}_n \in \mathbb{R}^{n\times n}$ with $\mathbf{C}_n^{i,j} = \frac{1}{2}(C(t_i',t_{j-1}) + C(t_i',t_j))$, $\mathbf{K}_n \in \mathbb{R}^n$ with $\mathbf{K}_n^i = K(t'_{i-\frac{1}{2}}, t_n)$, and $\mathbf{D}_n \in \mathbb{R}^n$ with $\mathbf{D}_n^i = D(t_{i-1}', t_n)$. If Eq. (5) is ill-conditioned, its solution would be unstable. The Tikhonov regularization is hence introduced, leading to the following regularized linear system:

$$(\Delta t^2 \mathbf{C}_n^T \mathbf{C}_n + \mu)\mathbf{K}_n = -\Delta t \mathbf{C}_n^T \mathbf{D}_n \,, \tag{6}$$

where $\mathbf{C}_n^T$ is the transpose of $\mathbf{C}_n$, and μ is the regularization parameter. The value of μ can be determined using the quasi-optimality criterion[31,32]. The detailed algorithm for determining the value of μ is provided in Supplementary Information. Note that the data of $D(t',t)$ may be obtained from $D(t',t) = \frac{\partial C(t',t)}{\partial t}$. The differentiation can be unstable and sensitive to the noise in the data of $C(t',t)$ and hence must be regularized as well, e.g., via discretization and the Tikhonov regularization[29,30].

Using the above method and the data of $C(t',t)$ for $0 \le t' \le t \le t_{\text{data}}$, we can determine the memory kernel $K(t',t)$ up to t_{data}. Compared with the iterative method proposed in[22], which recasts the nsGLE in a form where the memory kernel is expressed as a sum of convolution products and then determines each term recursively from the previous ones, our method is computationally more efficient and carefully addresses the ill-posedness of the problem.

In the case that we need to forecast the dynamics beyond the range of data, we can employ the Gaussian process regression (GPR) to extrapolate the memory kernel $K(t',t)$ up to t_{pred}, denoted as $K_{\text{pred}}(t',t)$. The furthest extrapolation time t_{pred} depends on the standard deviation (uncertainty level) of GPR. In particular, define $\mathbf{x} = [t',t]^T \in \mathbb{R}^2$ and $\mathbf{x}^* = [t'^*,t^*]^T \in \mathbb{R}^2$ as the inputs for training and prediction, respectively, with $0 \le t' \le t \le t_{\text{data}}$ and $0 \le t'^* \le t^* \le t_{\text{pred}}$. The Gaussian process model is given by: $K(t',t) \sim \mathscr{GP}[\mathbf{m}(\mathbf{x}), \mathbf{\Sigma}(\mathbf{x},\mathbf{x}^*)]$ with $\mathbf{m}(\mathbf{x})$ the mean function and $\mathbf{\Sigma}(\mathbf{x},\mathbf{x}^*)$ the covariance function. Here, the covariance function is assumed a squared exponential form with the hyper-parameters determined by minimizing the negative log marginal likelihood[33] via the Quasi-Newton optimizer L-BFGS[34]. A key advantage of GPR is that the uncertainty bounds of prediction can be derived from the hyper-parameters, and hence a measure for uncertainty at $t^* \ge t_{\text{data}}$ can be defined as:

$$\sigma^*(t^*) = \frac{\sum_{t'<t^*} |\hat{\sigma}(K_{\text{pred}}(t'^*,t^*))|^2}{\sum_{t'^*<t^*} |K_{\text{pred}}(t'^*,t^*)|^2} \,, \tag{7}$$

with $\hat{\sigma}(K_{\text{pred}}(t'^*,t^*))$ the standard deviation of GPR at $t^* > t_{\text{data}}$ for all $t'^* \le t^*$. From it we can determine the furthest extrapolation time t_{pred} by: $\sigma^*(t_{\text{pred}}) \le \zeta_{\text{GPR}}$, with ζ_{GPR} the desired tolerance of uncertainty in GPR.

2.2 Extended dynamics

After the memory kernel $K(t',t)$ is constructed, the next task is to specify the random noise term in Eq. (2), and we thus obtain an effective CG description in the form of nsGLE. The resulting nsGLE can then be solved to predict the non-equilibrium dynamics of the process. However, determining the random force from Eq. (3) is difficult. And directly solving Eq. (2) requires storing historical information and generating colored noise, which make it computationally expensive. To circumvent these difficulties, we first approximate the memory kernel $K(t',t)$ by an exponential expansion, noting that the memory is usually a decaying function generally with oscillations:

$$\begin{aligned} K(t',t) \approx \sum_{i=1}^{N} \alpha_i(t)\alpha_i(t') \exp(-\frac{a_i}{2}(t-t')) \\ [b_i \cos(q_i(t-t')) + c_i \sin(q_i(t-t'))] \,, \end{aligned} \tag{8}$$

where a_i, b_i, c_i and q_i are the parameters to be determined, satisfying $a_i \ge 0$, $b_i \ge 0$ and $|c_i| \le \frac{a_i b_i}{2q_i}$; and according to desired accuracy, N can be truncated to a finite number. Rewrite Eq. (8) into a matrix form:

$$K(t',t) = -\mathbf{A}_{ps}\boldsymbol{\alpha}(t) e^{-(t-t')\mathbf{A}_{ss}} \boldsymbol{\alpha}(t')\mathbf{A}_{sp} \,. \tag{9}$$

Here, $\boldsymbol{\alpha}(t) \in \mathbb{R}^{2N\times 2N}$ is a time-dependent parameter matrix composed of $\alpha_i(t)$; $\mathbf{A}_{ps} \in \mathbb{R}^{1\times 2N}$, $\mathbf{A}_{sp} \in \mathbb{R}^{2N\times 1}$, and $\mathbf{A}_{ss} \in \mathbb{R}^{2N\times 2N}$ are parameter matrices whose elements are comprised of the parameters: a_i, b_i, c_i and q_i in Eq. (8). The specific forms of the parameter matrices are provided in Supplementary Information. Given Eq. (9), the nsGLE in Eq. (2) is equivalent to the following extended dynamics, written for each dimension (P_k) of the CG variable $\mathbf{P}(t) \in \mathbb{R}^{d\times 1}$:

$$\begin{aligned} \begin{pmatrix} \dot{P}_k(t) \\ \dot{\mathbf{S}}_k(t) \end{pmatrix} = -\begin{pmatrix} \mathbf{0} & \mathbf{A}_{ps}\boldsymbol{\alpha}(t) \\ \boldsymbol{\alpha}(t)\mathbf{A}_{sp} & \mathbf{A}_{ss} \end{pmatrix} \begin{pmatrix} P_k(t) \\ \mathbf{S}_k(t) \end{pmatrix} \\ + \begin{pmatrix} \mathbf{0} & \mathbf{0} \\ \mathbf{0} & \mathbf{B}_s \end{pmatrix} \begin{pmatrix} 0 \\ \boldsymbol{\xi}(t) \end{pmatrix} \,, \end{aligned} \tag{10}$$

where $k = 1,2,\ldots,d$; $\mathbf{S}_k \in \mathbb{R}^{2N\times 1}$ is an auxiliary variable vector, whose initial state $\mathbf{S}_k(0)$ satisfies $\langle \mathbf{S}_k(0)\rangle = \mathbf{0}$ and $\langle \mathbf{S}_k(0)\mathbf{S}_k^T(0)\rangle = \frac{\langle |\mathbf{P}(t')|^2\rangle}{d}\mathbf{I}$; $\boldsymbol{\xi} \in \mathbb{R}^{2N\times 1}$ is a vector of uncorrelated Gaussian random variables with $\langle \xi_i(t)\rangle = 0$ and $\langle \xi_i(t)\xi_j(0)\rangle = \delta_{ij}\delta(t)$, where ξ_i and ξ_j denote the different elements of $\boldsymbol{\xi}$. The matrix $\mathbf{B}_s \in \mathbb{R}^{2N\times 2N}$ satisfies:

$$\mathbf{B}_s\mathbf{B}_s^T = \frac{\langle |\mathbf{P}(t')|^2\rangle}{d}(\mathbf{A}_{ss} + \mathbf{A}_{ss}^T) \,. \tag{11}$$

Each dimension of the random force in the nsGLE is given by:

$$\begin{aligned} \tilde{F}_k(t) = -\int_0^t \mathbf{A}_{ps}\boldsymbol{\alpha}(t) e^{-(t-t')\mathbf{A}_{ss}} \mathbf{B}_s \boldsymbol{\xi}(t')dt' \\ - \mathbf{A}_{ps}\boldsymbol{\alpha}(t) e^{-t\mathbf{A}_{ss}} \mathbf{S}_k(0) \,. \end{aligned} \tag{12}$$

The detailed proof of the equivalence of Eqs. (2) and (10) is provided in Supplementary Information. The nsGLE is hence converted to the extended dynamics that avoids convolution of mem-

ory and colored noise and hence is much cheaper to solve than the original nsGLE. A similar idea was proposed for solving the GLE in the context of equilibrium dynamics[9,12,35]. The present work represents the first attempt to generalize the framework of extended dynamics for non-stationary non-Markovian processes.

2.3 Parameterize the memory kernel

To determine the parameters in the expansion (Eq. (8)) approximating the memory kernel, we propose a data-driven optimization process. Rewrite Eq. (8) as $K(t',t) = \sum_{i=1}^{N} \alpha_i(t)\alpha_i(t')\beta_i(\tau)$ with $\beta_i(\tau) = \exp(-\frac{a_i}{2}\tau)[b_i\cos(q_i\tau) + c_i\sin(q_i\tau)]$, $\tau = t - t'$, and $\{a_i, b_i, c_i, q_i\} \in \boldsymbol{\lambda}_\beta$. Without prior knowledge, α_i can be approximated by a general polynomial as: $\alpha_i(t) = \sum_{j=0}^{M} p_{ij}t^j$, where M is the polynomial's order, and $\{p_{ij}\} \in \boldsymbol{\lambda}_\alpha$ are the coefficients. To determine the parameters $\boldsymbol{\lambda} = \{\boldsymbol{\lambda}_\alpha, \boldsymbol{\lambda}_\beta\}$, we solve the following optimization problem:

$$\boldsymbol{\lambda}^* = \arg\min_{\boldsymbol{\lambda}} \Pi(\boldsymbol{\lambda}) \,, \tag{13}$$

where $\Pi(\boldsymbol{\lambda})$ is the objective function and defined as: $\Pi(\boldsymbol{\lambda}) = \frac{\left\|K(t',t,\boldsymbol{\lambda}) - K_{\text{pred}}(t',t)\right\|_1}{\left\|K_{\text{pred}}(t',t)\right\|_1}$ with $\|\cdot\|_1$ the L_1 norm. Since $\Pi(\boldsymbol{\lambda})$ is generally non-convex, the optimization could easily fall into some local minima. Using different random initial guesses can alleviate this issue in some degree; however, it requires the numbers of initial guesses and independent optimization processes to increase exponentially with the dimension of $\boldsymbol{\lambda}$. Even for a moderately high-dimensional parameter space, the computational cost can be prohibitive. Thus, we employ a hybrid optimization process leveraging the differential evolution (DE)[36] and Levenberg–Marquardt (LM)[37,38] algorithms. The hybrid method is computationally efficient and can effectively avoid falling into local minima. In particular, the DE is used to narrow down appropriate initial guesses of $\boldsymbol{\lambda}$, and the LM is then used to find the nearby minimum.

Before the optimization process, we first determine the polynomial's order M in the approximation of $\alpha_i(t)$. Letting $t' = t$ in Eq. (8), we obtain $K(t,t) = \sum_{i=1}^{N} b_i\alpha_i^2(t)$. Since $K(t,t)$ is proportional to $\alpha_i^2(t)$, we can approximate $K(t,t)$ by a $2M$-order polynomial. Noting that any continuous function can be approximated by an expansion of Legendre polynomials[39], we next expand $K(t,t)$ with increasing order of Legendre polynomials. To proceed, we map $t \in [0, t_{\text{pred}}]$ to $\bar{t} \in [-1,1]$ by $\bar{t} = \frac{2t - t_{\text{pred}}}{t_{\text{pred}}}$ since Legendre polynomials are defined on the interval $[-1,1]$. $K(\bar{t},\bar{t})$ can then be expanded as:

$$K(\bar{t},\bar{t}) = \sum_{k=0}^{2M} \gamma_k L_k(\bar{t}) + \sum_{k=2M+1}^{\infty} \gamma_k L_k(\bar{t}) \,, \tag{14}$$

with $L_k(\bar{t})$ the kth-order Legendre polynomial basis. The coefficient γ_k can be determined from[39]:

$$\gamma_k = \frac{2k+1}{2} \int_{-1}^{1} K(\bar{t},\bar{t}) L_k(\bar{t}) d\bar{t} \,, \tag{15}$$

where the integral can be numerically evaluated by a quadrature rule, e.g., the trapezoidal rule. Due to the orthonormality and completeness of the Legendre polynomials, the terms $\sum_{k=2M+1}^{\infty} \gamma_k L_k(\bar{t})$ can be neglected in Eq. (14) given the tolerance of truncation error. By such, we can determine the polynomial's order M in the approximation of $\alpha_i(t)$. After that, we proceed with the hybrid optimization process based on the DE and LM algorithms to solve the optimization problem in Eq. (13).

The DE is a type of evolutionary algorithm for global optimization[36], whose basic idea is to reduce the objective function by generating mutated vectors, usually called greedy search. Greedy search converges fast but can be trapped by some local minima. The DE overcomes this difficulty by simultaneously generating several vectors (called population), where mutation is achieved by comparing two vectors and then adding their difference after weighted to a third vector. The population and mutation ensure a thorough exploration over the searching space and avoid falling into a local minimum. Thus, the DE is potentially capable to solve the global optimization problems that are non-differentiable and have multiple local minima[40]. Its key specifics are provided below. First, the DE draws on a population of individuals, which are defined as the $\mathscr{D}$-dimensional parameter vectors $\boldsymbol{\lambda}_{g,k}$ for $k = 1,2,...,NP$, where $\mathscr{D} = N(M+5)$, NP is the population size, and g represents the generation. All individuals are randomly initialized as $\boldsymbol{\lambda}_{0,k}$ over the searching space. Unless stated otherwise, we assume a uniform probability distribution for all random samplings. Second, the following steps are iterated until the stopping criterion of optimization (based on the maximum number of iterations $g_{\max}$ or the desired tolerance) is met.

1) Mutation: For each individual $\boldsymbol{\lambda}_{g,k}$, $k = 1,2,\ldots,NP$, a mutant vector is generated according to

$$\mathbf{v}_k = \boldsymbol{\lambda}_{g,k_1} + F_M \cdot (\boldsymbol{\lambda}_{g,k_2} - \boldsymbol{\lambda}_{g,k_3}) \,, \tag{16}$$

where $k_1, k_2, k_3 \in [1, NP]$ are randomly chosen and distinct from each other; $F_M > 0$ is a scaling factor that controls the mutation, which is called the mutation weight.

2) Crossover: A trial vector $\mathbf{u}_k$ is created by:

$$\mathbf{u}_k(l) = \begin{cases} \mathbf{v}_k(l), & \omega_l < CR \\ \boldsymbol{\lambda}_{g,k}(l), & \omega_l \geq CR \end{cases} \,, \tag{17}$$

where $\omega_l \in [0,1]$ is a uniformly distributed random number for $l = 1,2,\ldots,\mathscr{D}$, and $CR \in [0,1]$ is the preset crossover rate.

3) Selection: To decide whether or not the trial vector $\mathbf{u}_k$ should become an individual of the next generation, it is compared with the original vector $\boldsymbol{\lambda}_{g,k}$ by a greedy selection:

$$\boldsymbol{\lambda}_{g+1,k} = \begin{cases} \mathbf{u}_k, & \Pi(\mathbf{u}_k) < \Pi(\boldsymbol{\lambda}_{g,k}) \\ \boldsymbol{\lambda}_{g,k}, & \Pi(\mathbf{u}_k) \geq \Pi(\boldsymbol{\lambda}_{g,k}) \end{cases} \,, \tag{18}$$

where $\boldsymbol{\lambda}_{g+1,k}$ is the offspring of $\boldsymbol{\lambda}_{g,k}$ for the next generation. The values of the population size NP, mutation weight F_M, and crossover rate CR are set following Gämperle[41].

Although the DE has demonstrated its superior performance, e.g. robustness and fast convergence, by numerical experiments for solving benchmark global optimization problems with dimensions up to 100[42], its computational cost could enormously increases when refining the solution since it does not use the infor-

mation of gradients. As a result, it is challenging for the DE to accurately determine the precise position of optimum with reasonable computational cost. Therefore, we propose a hybrid method combining the DE with a robust local optimization algorithm, the LM[37]. To proceed, we set a tolerance $\zeta_{\rm DE}$ for the DE, which is larger than the desired tolerance $\zeta_{\rm opt}$ for the entire optimization. When the minimum of the objective function for the current generation in the DE $\Pi(\boldsymbol{\lambda}_g^*)$ is smaller than that of the last generation and also the preset tolerance $\zeta_{\rm DE}$, $\boldsymbol{\lambda}_g^*$ is taken as the starting point for the LM algorithm to search the nearby local minimum $\boldsymbol{\lambda}^*$. If $\Pi(\boldsymbol{\lambda}^*) \leq \zeta_{\rm opt}$, the optimization process is terminated, and we find the optimal parameters $\boldsymbol{\lambda}^* = \{\boldsymbol{\lambda}_\alpha^*, \boldsymbol{\lambda}_\beta^*\}$; otherwise, we return to the DE and proceed to the next generation. The detailed algorithm of the hybrid optimization is outlined in Algorithm 1.

Algorithm 1 Hybrid optimization

Require: Memory kernel data of $K_{\rm pred}(t',t)$ with $0 \leq t' \leq t \leq t_{\rm pred}$
Ensure: Optimized parameters $\boldsymbol{\lambda}^*$
for $N = 1,2,\ldots$ **do**
  Initialize NP random parameter vectors $\boldsymbol{\lambda}_{0,k}$ with $k = 1,2,...,NP$ and set $\zeta = \min\{\Pi(\boldsymbol{\lambda}_{0,1}), \Pi(\boldsymbol{\lambda}_{0,2}), \ldots, \Pi(\boldsymbol{\lambda}_{0,NP})\}$
  for $g = 0,1,\ldots,g_{\max}$ **do**
    $\boldsymbol{\lambda}_g^* = \underset{k=1,2,...,NP}{\arg\min}\ \{\Pi(\boldsymbol{\lambda}_{g,k})\}$
    if $\Pi(\boldsymbol{\lambda}_g^*) < \min(\zeta_{\rm DE}, \zeta)$ **then**
      $\zeta = \Pi(\boldsymbol{\lambda}_g^*)$
      Search $\boldsymbol{\lambda}^*$ by the LM with $\boldsymbol{\lambda}_g^*$ as the starting point
      if $\Pi(\boldsymbol{\lambda}^*) < \zeta_{\rm opt}$ **then**
        Output $\boldsymbol{\lambda}^*$ and terminate all loops
      end if
    end if
    for $k = 1,2,...,NP$ **do**
      Generate a mutant vector $\mathbf{v}_k$ by Eq. (16)
      Create a trial vector $\mathbf{u}_k$ by Eq. (17)
      Make the next generation $\boldsymbol{\lambda}_{g+1,k}$ by Eq. (18)
    end for
  end for
end for
return $\boldsymbol{\lambda}^*$

3 Numerical example

As a proof of principle, we applied the proposed methodology to a benchmark non-equilibrium problem: heating a star-polymer melt. The CG coordinate was chosen at the center of mass (COM) of a tagged star polymer immersed in the melt of other identical star polymers. The momentum (normalized) of the COM of the tagged star polymer was the CG variable. We analyzed the non-equilibrium dynamics of this tagged star polymer during the heating process and constructed the dynamic equation of the CG variable based on the nsGLE. The data of the reference high-dimension Hamiltonian system were obtained from MD simulations, and hence, while one set of MD simulation results were used to construct the CG dynamic equation, the other set was used for validating the CG modeling predictions. In particular, we collected the data of the two-time auto-correlation function of momentum $C(t',t) = \langle \mathbf{P}(t') \cdot \mathbf{P}(t) \rangle$ from MD simulations. The constructed nsGLE was solved via the extended dynamics, whose predictions within or outside the range of data set used to construct the CG model were compared with the MD simulation results. All of the simulations were performed using LAMMPS[43].

The star-polymer melt consists of 1,000 identical star polymers including the tagged one. In the MD simulation, each star polymer consists of 31 Lennard-Jones (LJ) beads, i.e. a core LJ bead and 10 identical arms with 3 LJ beads per arm. The core LJ bead and the LJ beads in each arm are connected by the finitely extensible non-linear elastic (FENE) bonds. The dynamics of the atomistic system is governed by the Hamiltonian:

$$H = \sum_{i=1}^{n_a} \frac{\mathbf{p}_i^2}{2m_i} + \sum_{i \neq j} E(r_{ij}) \,, \tag{19}$$

where n_a is the total number of LJ beads in the atomistic system; $\mathbf{p}_i$ and m_i are the momentum and mass of the i-th LJ bead, respectively; $r_{ij} = |\mathbf{r}_{ij}| = |\mathbf{r}_i - \mathbf{r}_j|$ is the distance between two LJ beads; and E denotes the total potential energy contributed by the inter-atomic and bonded potentials. The inter-atomic LJ potential adopts the purely repulsive Weeks-Chandler-Andersen (WCA) potential and is given by:

$$E_{\rm WCA}(r) = \begin{cases} 4\varepsilon[(\frac{\sigma}{r})^{12} - (\frac{\sigma}{r})^6 + \frac{1}{4}] & r \leq r_c \\ \infty & r > r_c \end{cases} , \tag{20}$$

where $r_c = 2^{1/6}\sigma$ is the cutoff distance. The FENE potential for the bonded interaction between connected LJ beads is:

$$E_{\rm FENE}(r) = \begin{cases} -\frac{1}{2} k_b r_0^2 \ln[1 - (\frac{r}{r_0})^2] & r \leq r_0 \\ \infty & r > r_0 \end{cases} , \tag{21}$$

where $k_b = 3000\varepsilon/\sigma^2$ is the spring constant, and $r_0 = 1.5\sigma$ is the maximum length of the FENE spring. The mass of all LJ beads was chosen to be unity. The simulation box was a periodic cubic box of length 33.8395σ. The reduced LJ units were used herein; i.e., the units of mass, length, and energy are set as: $m = 1$, $\sigma = 1$, and $\varepsilon = 1$, and the corresponding unit of time is $\sigma(m/\varepsilon)^{0.5} = 1$. The Nose-Hoover thermostat under the canonical ensemble (NVT) with the thermostat relaxation time 0.6 was employed with the time step $\Delta t = 0.001$. The MD simulation was first performed at $k_BT = 1.0$ for 10^6 time steps to equilibrate the system and then continued with the temperature continuously rising from $k_BT = 1$ to $k_BT = 2$ for 15,000 time steps from $t = 0.0$ to $t = 15.0$. From the MD simulations, 8,000 independent trajectories were collected to obtain the data of $C(t',t)$ (see Fig. 1), from which the CG model was constructed. In addition, we collected 120,000 more independent trajectories to obtain the corresponding $C(t',t)$ as the reference for validating the CG modeling predictions.

3.1 Compute the memory kernel from data

To determine the memory kernel $K(t',t)$ from the data of $C(t',t)$, the force-momentum correlation function $D(t',t) = \frac{\partial C(t',t)}{\partial t}$ was first computed via numerical differentiation regularized by the Tikhonov regularization following the quasi-optimality principle (see Supplementary Information) with $\mu_0 = 0.1$ and $\eta = 0.99$.

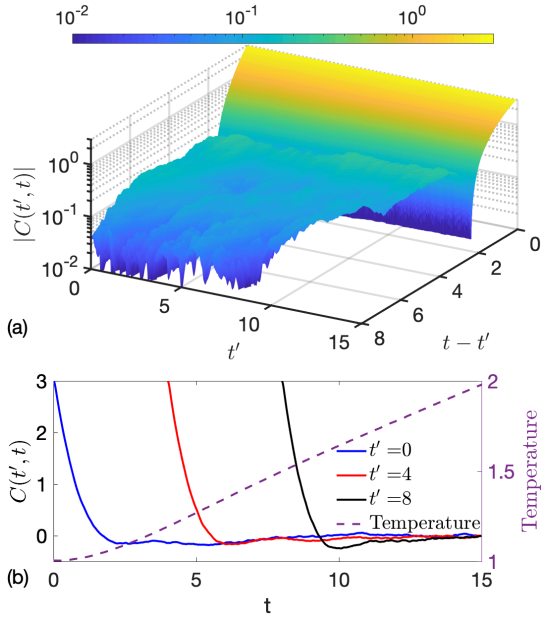

Fig. 1 Data of $C(t',t)$ obtained from the MD simulations. (a) 3-D view as a function of $t-t'$ and t', where the data are shown in absolute values. (b) Dependence of $C(t',t)$ on t at different t' (solid lines), along with the temperature (k_BT) as a function of t (dashed line).

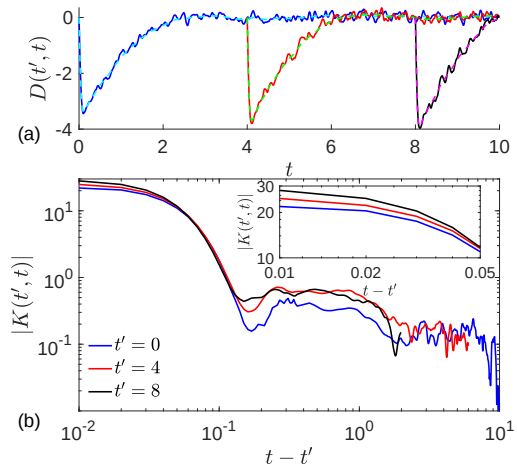

Fig. 2 (a) $D(t',t)$ obtained via direct numerical differentiation (solid lines) vs. via regularized numerical differentiation by the Tikhonov regularization (dashed lines). (b) The absolute value of $K(t',t)$ (on a logarithmic scale) computed from Eq. (5) using the data of $C(t',t)$ and regularized $D(t',t)$. The zoom-in subplot provides a closer view of $|K(t',t)|$ for $0 \le t-t' \le 0.05$. All the results herein are plotted at $t'=0$, $t'=4$, and $t'=8$.

With the discrete data of $C(t',t)$ and $D(t',t)$ obtained, Eq. (5) was not ill-conditioned and hence was directly solved for $K(t',t)$ up to t_{data}. Fig. 2 presents the resulting $D(t',t)$ and $K(t',t)$.

3.2 Extrapolate the memory kernel

The memory kernel $K(t',t)$ computed from the MD simulation data was then extrapolated by the GPR for longer time prediction beyond t_{data} until t_{pred}. For this numerical example, the following modified squared exponential function was employed as the covariance function:

$$\Sigma(\mathbf{x},\mathbf{x}^*;\boldsymbol{\theta}) = \theta_f^2 \exp\left[-\frac{(t-t^*)^2}{2\theta_{l_1}^2} - \frac{(t-t'-t^*+t'^*)^2}{2\theta_{l_2}^2}\right],$$

where $\boldsymbol{\theta} = [\theta_f, \theta_{l_1}, \theta_{l_2}]$ are the hyper-parameters. The predicted memory kernel, K_{pred}, is shown in Fig. 3, where $t_{\text{data}} = 10$, $t_{\text{pred}} = 12$, and the tolerance of the GPR uncertainty was set as $\zeta_{\text{GPR}} = 0.008$. We further compared the GPR's predictions with the test data and assessed the relative error:

$$\varepsilon_r(t^*) = \frac{\sum_{t'^* \le t^*} |K_{\text{pred}}(t'^*,t^*) - K(t'^*,t^*)|^2}{\sum_{t'^* \le t^*} |K(t'^*,t^*)|^2}$$

and the uncertainty level of GPR $\sigma^*(t^*)$ (defined in Eq. (7)) at different prediction times $10 < t^* \le 15$. For that, $K_{\text{pred}}(t'^*,t^*)$ was predicted by GPR using the training data within $0 \le t' \le t \le 10$; the test data $K(t'^*,t^*)$ for $10 < t'^* \le t^* < 15$ was obtained by solving Eq. (5) with the data of $C(t'^*,t^*)$. From the results depicted in Fig. 4, we can see that as the extrapolation time goes further, the uncertainty level $\sigma^*(t^*)$ and the relative error $\varepsilon_r(t^*)$ both increase with similar trends, which also supports the use of $\sigma^*(t^*)$ as a criterion to determine from data the furthest prediction time t_{pred}.

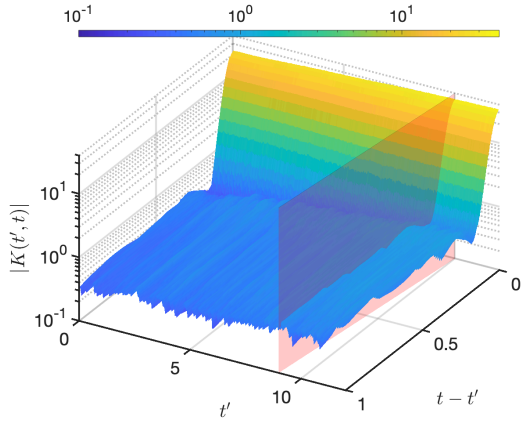

Fig. 3 Predicted memory kernel $K_{\text{pred}}(t',t)$ by the GPR model. Here, $K_{\text{pred}}(t',t)$ is divided into two parts by a red vertical flat surface: the left corresponds to the regression from the training data for $0 \le t' \le t \le t_{\text{data}} = 10$; the right corresponds to the extrapolation from the training data for $t_{\text{data}} < t' \le t \le t_{\text{pred}} = 12$.

More investigations were performed for assessing the ability of GPR to extrapolate the memory kernel when using different sets of training data. Specifically, three sets of data within $0 \le t' \le t \le 2$ (Set 1), $4 \le t' \le t \le 6$ (Set 2), and $8 \le t' \le t \le 10$ (Set 3), respectively, were compared. Fig. 5 summaries the computed uncertainty of GPR $\sigma^*(t^*)$ when using the three sets of training data for prediction of the memory kernel at different extrapolation times $t^* > t_{\text{data}}$.

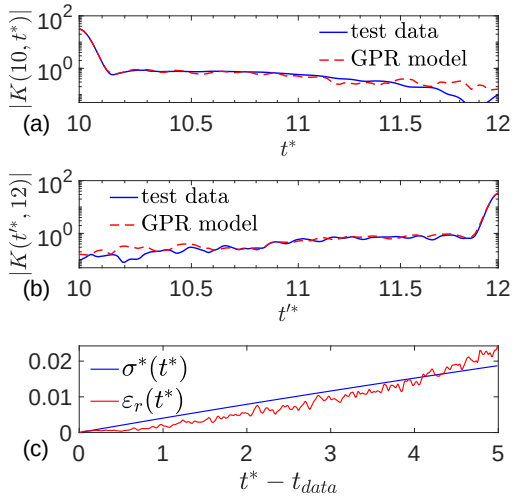

Fig. 4 (a) and (b) Comparison of the GPR model's predictions with the test data at $t'^* = 10$ and $t^* = 12$, respectively. (c) The relative error $\varepsilon_r(t^*)$ and the uncertainty level $\sigma^*(t^*)$ of GPR at different extrapolation times $t^* > t_{\text{data}}$.

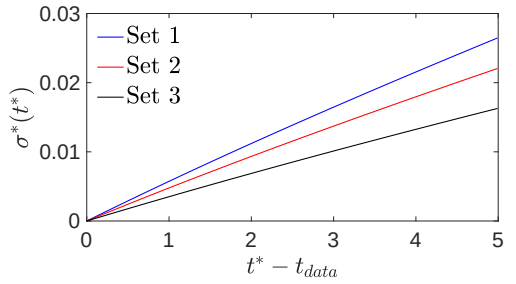

Fig. 5 Uncertainty of GPR $\sigma^*(t^*)$ in the prediction of the memory kernel for $t^* > t_{\text{data}}$ using different sets of training data.

Although each set has the same amount of data, the prediction based on each exhibits different uncertainty at the same $t^* - t_{\text{data}}$. Using the data in earlier times resulted in larger uncertainty in prediction. It can be due to the fact that the heating process considered in this work displayed nonlinear temperature rises in earlier times, which led to more complex variations in the memory kernel as a function of time in earlier times than later. Thus, how far the memory kernel can be extrapolated depends on the choice of training data as well as the desired tolerance of uncertainty.

3.3 Parameterize the memory kernel

The parameterization of $K_{\text{pred}}(t',t)$ was achieved using the proposed hybrid optimization process, from which the approximation of $K_{\text{pred}}(t',t)$ via the expansion in Eq. (8) was constructed with $M = 2$ and $N = 4$. The tolerance of optimization was set as $\zeta_{\text{opt}} = 0.1$, and the value of the objective function corresponding to the optimal parameters is $\Pi(\boldsymbol{\lambda}^*) = 0.092$. The values of other parameters involved in the hybrid optimization were set as: $NP = 10\mathscr{D}$, $F_M = 0.8$, $CR = 0.5$, $g_{\max} = 1e^6$, $\zeta_{\text{DE}} = 0.5$, and $\zeta_{\text{opt}} = 0.1$. The searching space of $\boldsymbol{\lambda}$ was set with: $p_{ij} \in [-1,+1]$, $a_i \in [0,100]$, $b_i \in [0,100]$, $q_i \in [0,100]$, and $c_i \in [-\frac{a_i b_i}{2q_i}, \frac{a_i b_i}{2q_i}]$, which is as large as physically reasonable.

The predicted and parameterized memory kernels are compared in Fig. 6. The parameterized memory kernel $K_{\text{param}}(t',t)$ with $N = 3$ is also shown. Note that the accuracy of approximating the memory kernel via the two-time exponential expansion increases by truncating the expansion with more terms, i.e., increasing N. Thus, the parameterization with larger N is more accurate.

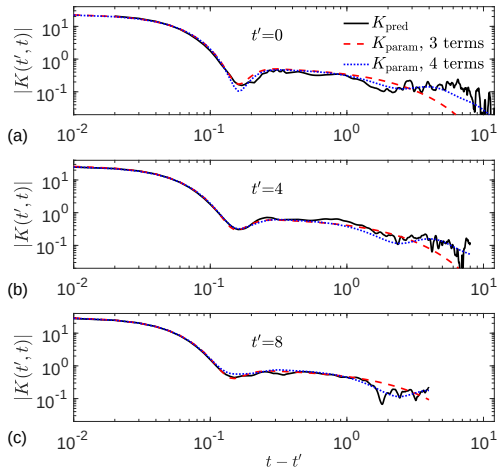

Fig. 6 The parameterized memory kernel $K_{\text{param}}(t',t)$ with $N = 3$ or $N = 4$, compared with the predicted memory kernel $K_{\text{pred}}(t',t)$ at different t'.

3.4 CG modeling predictions

From the parameterized memory kernel and Eq. (9), we assembled the matrices $\boldsymbol{\alpha}(t)$, $\mathbf{A}$, and $\mathbf{B}_s$ for the extended dynamics. The CG modeling predictions until t_{pred} were obtained by solving Eq. (10) using the implicit velocity-Verlet temporal integrator. The two-time auto-correlation function of momentum $C(t',t)$ predicted by the CG model was compared with the MD simulation results, as depicted in Fig. 7. We found good agreements. And the CG model constructed using the parameterized memory kernel with larger N is more accurate. The relative error between the CG (with $N = 4$) prediction and the reference MD result is: $\frac{\|C_{\text{CG}}(t',t) - C_{\text{MD}}(t',t)\|_1}{\|C_{\text{MD}}(t',t)\|_1} = 0.03$, where $\|\cdot\|_1$ denotes the L_1 norm of discrete data; the data of $C_{\text{CG}}(t',t)$ and $C_{\text{MD}}(t',t)$ were attained from the CG and MD simulations, respectively.

4 Conclusion

We have presented a data-driven approach for constructing CG models of Hamiltonian systems in non-equilibrium dynamics. It goes beyond existing literature in CG modeling, which mainly focuses on how to properly describe the equilibrium dynamics of CG variables. Our approach has addressed the key challenges in CG modeling of non-equilibrium systems, including how to efficiently and stably determine the non-stationary memory kernel, how to give an explicit form of the random noise such that the memory and random noise satisfy the non-stationary

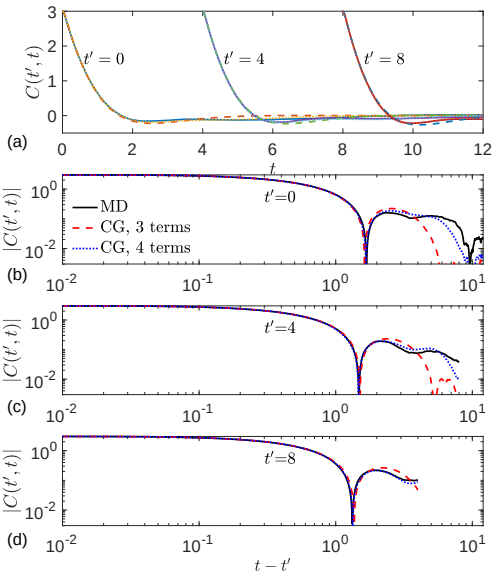

Fig. 7 $C(t',t)$ predicted by the CG model constructed from the parameterized memory kernel with $N=3$ (dashed line) or $N=4$ (dotted line), respectively, compared with the MD simulation results (solid line) at different t'. (a) $C(t',t)$ on a linear scale. (b) $\sim$ (d) The absolute value of $C(t',t')$ on a logarithmic scale.

fluctuation-dissipation relation, and how to efficiently solve the non-stationary dynamic equation of CG variables. Through the numerical example, we have demonstrated that the CG model can predict with desired accuracy the non-equilibrium dynamics of the observable of interest both inside and outside the regime of data used to construct the CG model. The approach only requires the data of the two-time auto-correlation function of non-equilibrium trajectory-averaged observable of interest, which can be readily obtained from simulations or experiments. We anticipate that the methodology proposed in this work can be generally applied to modeling high-dimensional non-equilibrium dynamics in reduced dimensions for various soft matter systems such as polymers, biomolecules, and colloids.

Conflicts of interest

There are no conflicts to declare.

Acknowledgements

This material is based upon work supported by the Defense Established Program to Stimulate Competitive Research (DEPSCoR) Grant No. FA9550-20-1-0072 and by the National Science Foundation under Grant No. CMMI-1761068.

References

1 P. C. Souza, S. Thallmair, P. Conflitti, C. Ramírez-Palacios, R. Alessandri, S. Raniolo, V. Limongelli and S. J. Marrink, *Nature communications*, 2020, **11**, 1–11.

2 S. Kmiecik, D. Gront, M. Kolinski, L. Wieteska, A. E. Dawid and A. Kolinski, *Chemical reviews*, 2016, **116**, 7898–7936.

3 O. F. Lange and H. Grubmüller, *The Journal of Chemical Physics*, 2006, **124**, 214903.

4 H. Meyer, T. Voigtmann and T. Schilling, *The Journal of chemical physics*, 2019, **150**, 174118.

5 H. Mori, *Progress of Theoretical Physics*, 1965, **33**, 423–455.

6 R. Zwanzig, *Phys. Rev.*, 1961, **124**, 983–992.

7 Z. Li, X. Bian, X. Li and G. E. Karniadakis, *The Journal of Chemical Physics*, 2015, **143**, 243128.

8 H. Lei, N. A. Baker and X. Li, *Proceedings of the National Academy of Sciences*, 2016, **113**, 14183–14188.

9 Z. Li, H. S. Lee, E. Darve and G. E. Karniadakis, *The Journal of chemical physics*, 2017, **146**, 014104.

10 G. Jung, M. Hanke and F. Schmid, *Soft matter*, 2018, **14**, 9368–9382.

11 H. S. Lee, S.-H. Ahn and E. F. Darve, *The Journal of Chemical Physics*, 2019, **150**, 174113.

12 S. Wang, Z. Li and W. Pan, *Soft matter*, 2019, **15**, 7567–7582.

13 S. Wang, Z. Ma and W. Pan, *Soft Matter*, 2020, **16**, 8330–8344.

14 W. M. Jacobs, A. Reinhardt and D. Frenkel, *Proceedings of the National Academy of Sciences*, 2015, **112**, 6313–6318.

15 M. Sajfutdinow, W. M. Jacobs, A. Reinhardt, C. Schneider and D. M. Smith, *Proceedings of the National Academy of Sciences*, 2018, **115**, E5877–E5886.

16 K. W. Tan, B. Jung, J. G. Werner, E. R. Rhoades, M. O. Thompson and U. Wiesner, *Science*, 2015, **349**, 54–58.

17 V. Krieger, E. Ciglia, R. Thoma, V. Vasylyeva, B. Frieg, N. de Sousa Amadeu, T. Kurz, C. Janiak, H. Gohlke and F. K. Hansen, *Chemistry A European Journal*, 2017, **23**, 3699–3707.

18 S. R. Quake, H. Babcock and S. Chu, *Nature*, 1997, **388**, 151–154.

19 T. T. Perkins, D. E. Smith and S. Chu, *Science*, 1997, **276**, 2016–2021.

20 H. Meyer, T. Voigtmann and T. Schilling, *The Journal of chemical physics*, 2017, **147**, 214110.

21 H. Grabert, *Projection operator techniques in nonequilibrium statistical mechanics*, Springer, 1982.

22 H. Meyer, P. Pelagejcev and T. Schilling, *Europhysics Letters*, 2020, **128**, 40001.

23 P. Español and P. B. Warren, *The Journal of Chemical Physics*, 2017, **146**, 150901.

24 C. Hijón, P. Espanõl, E. Vanden-Eijnden and R. Delgado-Buscalioni, *Faraday Discuss.*, 2010, **144**, 301–322.

25 R. Kubo, *Reports on Progress in Physics*, 1966, **29**, 255–284.

26 P. Linz, *Analytical and Numerical Methods for Volterra Equations*, Society for Industrial and Applied Mathematics (SIAM), Philadelphia, PA, 1985.

27 P. K. Lamm, *Surveys on Solution Methods for Inverse Problems*, Springer, Vienna, 2000, pp. 53–82.

28 C. Groetsch, *Handbook of Mathematical Methods in Imaging*, Springer, New York, 2015, pp. 3–41.

29 A. N. Tikhonov, *Soviet Mathematics Doklady*, 1963, **4**, 1624–1627.

30 A. N. Tikhonov, *Soviet Mathematics Doklady*, 1963, **4**, 1035–1038.
31 A. N. Tikhonov and V. B. Glasko, *USSR Computational Mathematics and Mathematical Physics*, 1964, **4**, 236–247.
32 A. N. Tikhonov and V. B. Glasko, *USSR Computational Mathematics and Mathematical Physics*, 1965, **5**, 93–107.
33 C. K. Williams and C. E. Rasmussen, *Gaussian processes for machine learning*, MIT press Cambridge, MA, 2006, vol. 2.
34 D. C. Liu and J. Nocedal, *Mathematical programming*, 1989, **45**, 503–528.
35 M. Ceriotti, G. Bussi and M. Parrinello, *Journal of Chemical Theory and Computation*, 2010, **6**, 1170–1180.
36 R. Storn and K. Price, *Journal of Global Optimization*, 1997, **11**, 341–359.
37 K. Levenberg, *Quarterly of applied mathematics*, 1944, **2**, 164–168.
38 C. Kanzow, N. Yamashita and M. Fukushima, *Journal of Computational and Applied Mathematics*, 2004, **172**, 375 – 397.
39 M. Abramowitz and I. A. Stegun, *Handbook of mathematical functions with formulas, graphs, and mathematical tables*, US Government printing office, 1970, vol. 55.
40 K. V. Price, *New Ideas in Optimization*, McGraw-Hill, London, 1999, pp. 77–106.
41 R. Gämperle, S. D. Müller and P. Koumoutsakos, WSEAS Int. Conf. on Advances in Intelligent Systems, Fuzzy Systems, Evolutionary Computation, 2002, pp. 293–298.
42 J. Vesterstrom and R. Thomsen, Proceedings of the 2004 Congress on Evolutionary Computation, 2004, pp. 1980–1987.
43 S. Plimpton, *Journal of computational physics*, 1995, **117**, 1–19.